Journal of Imaging Science and Technology® 54(6): 060501–060501-9, 2010.

Behavior of Charged Particles Around a Wire in a Scorotron on Negative Corona Discharge

Kazuhiro Mori
Key Technology Laboratory, Research and Technology Group, Fuji Xerox Co., Ltd., Nakai-machi, Ashigarakami-gun, Kanagawa 259-0157, Japan
E-mail: kazuhiro.mori@fujixerox.co.jp

Abstract. *The existence of charged particles in corona devices is important in electrophotography. Envelope regions where introduced smoke particles cannot penetrate appear around wires on corona discharge in spite of the polarization of the wires. These particles that are initially positive charged keep away from around the wire and collide with the grid electrode on negative corona discharge. With knowledge of particle charging the author shows the motion of charged particles around a corona wire. Numerical calculations correlate well with experimental results. The author defines the generation process of these regions by comparing the initial flow field with numerical simulation results. In addition, the charge quantity of the smoke particles is estimated. © 2010 Society for Imaging Science and Technology.*
[DOI: 10.2352/J.ImagingSci.Technol.2010.54.6.060501]

INTRODUCTION

Corona discharge is used in charging processes in electrophotography.[1] Although corona discharge may be considered a classic technology, corona devices are still used in high-speed machines. On corona discharge, ionic wind occurs by the Coulomb force exerted on ions and collisions of ions and neutral molecules of gas. Ions collide with the molecules of the air, and transfer the momentum to the air. The ionic wind transports oxidation products etc., which causes image degradation and environmental problems.

Many investigations of corona discharge including the ionic wind have been conducted.[2–6] In electrophotography, Nashimoto[5] reported the fundamental investigations of silicon oxide growth and reactive gas generation induced by corona discharge, and presented the means to compensate for these phenomena. Zamankhan and co-workers[6] have studied similar problems two-dimensionally using coupled systems of electric and hydrodynamic governing equations. In previous articles,[7–9] we reported basic characteristics of the ionic wind in a single-wire and a double-wire scorotron. A primary flow appears in cross-section, and several vortices are induced by the primary flow. Our numerical calculations correlated well with our experimental results by particle image velocimetry (PIV). The primary flow appears also in cross-section in a pull ventilation system, while the flow rate of the whole system is hardly changed. Hence, the primary flow in a single-wire scorotron is a λ-shaped flow. We could determine that this primary flow is derived from the schematic distribution of the body force. The ionic wind influences the flow field in the neighborhood of the corona device.

Scharfe stated that it is difficult to control and maintain free powders[10] as early as 1984. Free powders cause contamination in machinery, so we are happy if there are no free powders and chemical species in precision machinery. Unfortunately there are several unknown phenomena. Do free powders contaminate a grid on corona discharge? Free powders may contaminate a grid and, after corona discharge, they may contaminate the wire. No one has distinguished free powders from chemical species as contamination sources. Otsuka and Shiraishi[11] reported that dusts carried onto the wire surface by airflow caused excessive discharge at the point of deposit, which thinned the wire. They prevented the recurrence of the failure by changing the airflow system and the material of the wire. Thus polluted substances may unevenly contaminate a corona device. It is a reasonable conclusion that such contamination is related to image degradation. Small powders move on airflow. Managing airflow and inflow of the polluted substances to corona devices is significant for preventing image degradation.[12] So we have first investigated the flow field that has a close relationship to contamination.

In the previous article,[9] we reported that envelope regions appear downstream of the wire in a double-wire scorotron on negative corona discharge. Images of introduced smoke particles implicitly show a significant possibility that certain free powders do not contaminate a wire on corona discharge. We showed the calculated behavior of charged particles in the double-wire scorotron. Yoshizawa and co-workers[13] independently showed a similar image on positive corona discharge. Envelope regions that the introduced smoke particles cannot penetrate appear on corona discharge in spite of the polarization of the wires.

Contamination engineering is a new field and in electrophotography, contamination engineering has not yet been established. Chemical reactions such as chemical vapor deposition (CVD) may govern the contamination of the wire on corona discharge. After corona discharge, however, free powders may contaminate the wire. Therefore, knowledge of physical phenomena in the neighborhood of corona

Received Dec. 23, 2009; accepted for publication Aug. 6, 2010; published online Nov. 4, 2010.
1062-3701/2010/54(6)/060501/9/$20.00.

devices is necessary. Using a high-speed camera Hoshino and co-workers[14] observed the motion of the particles made of several kinds of materials between voltage-applied electrodes. However, the motion of the particles in a corona device has never been shown. So we have investigated the motion of some charged particles in a corona device on corona discharge. As we have no visualization method for the motion of particles other than smoke particles, we therefore have to discuss the motion of smoke particles in this article.

Corona devices have great variety. Airflow systems around corona devices also have great variety. In this article we report the motion of smoke particles in a double-wire scorotron on negative corona discharge. The next section discusses the analysis model and numerical conditions. The third section describes the electric field and flow field calculations: First, we use a computer program FLUENT Ver. 6.3.26 (FLUENT Inc., Lebanon, NH, USA) to calculate the electric field with the two-dimensional corona discharge simulation. Next, FLUENT calculates the steady two-dimensional flow field with a two-dimensional fine mesh.

We then illustrate a two-dimensional flow field by smoke particles on negative corona discharge. Smoke particles show that a long envelope region appears after decay of an elliptical region. From this imagery we derive velocity vectors, contours of static pressure, and the behavior of uniformly charged smoke particles. Our numerical calculations qualitatively correlate well with our experimental results. Since the existence of charged particles in corona devices is important in electrophotography, we next estimate particle charge under the influence of the electric field strength, which is a local function. Finally, we summarize the motion of the charged particles around a wire in the double-wire scorotron.

TWO-DIMENSIONAL ANALYSIS MODEL AND CONDITIONS FOR NUMERICAL CALCULATIONS

Since we investigate the basic characteristics of the ionic wind in this paper, our studies have focused on the flow field in the neighborhood of the scorotron. A scorotron is one type of corona device with a grid to control corona charging. Figure 1(a) shows the scorotron and the photoreceptor. The scorotron is depicted as a rectangular solid attached to the cylindrical photoreceptor. The photoreceptor rotates counterclockwise at 0.5 m/s. The scorotron has insulator blocks on both ends to stretch a wire electrode. Fig. 1(b) shows a two-dimensional analysis model. The axial direction of the wire is vertical. Space around a scorotron was set widely, i.e., we assumed a scorotron and a photoreceptor in open space. The outer surfaces provide the pressure outlet boundary. This model has about 240 000 quadrilateral cells. The analysis model consists of a two-dimensional surface, with cross-sectional dimensions of 100×80 mm^2.

In addition, a cross section in the neighborhood of the scorotron is shown in Fig. 1(c). There is a slit on the ceiling of the shield electrode for ventilation. The grid is set between the wire and the photoreceptor. The inner part of the scorotron is separated into two parts by a central shield electrode. Two wire electrodes are stretched in the inner of the metal shield electrode. Both wire electrodes are offset 1 mm to the left from the front view. The wire at the upstream side and the wire at the downstream side, are called the first wire and the second wire, respectively. A grid electrode is set between the wire electrode and photoreceptor to help uniform charging. Figs. 1(d) and 1(e) show computational meshes. Table I shows geometrical parameters for the scorotron and the photoreceptor. Table II shows electrical parameters for the scorotron and the photoreceptor.

We have considered the negative corona discharge whereby electrons are emitted from the wire. For simplicity, a numerical simulation is described by the positive value of the voltage and the charge density. Numerical results are consistent in spite of the polarization of the electrodes.

ELECTRIC FIELD AND FLUID CALCULATIONS

The ionic wind is a complex phenomenon.[2] The electric field, flow field, and temperature field mutually affect one another. Since the electrostatic force to the air is dominant, other effects are considered to be negligible in this analysis. Electrostatic force is calculated from the distribution of the electric field and charge density. These distributions are obtained by solving Gauss' Law

$$\frac{\partial(\varepsilon_{ij}E_j)}{\partial x_i} = \rho_e, \tag{1}$$

and the charge conservation equation

$$\frac{\partial \rho_e}{\partial t} + \frac{\partial(\mu_e \rho_e E_j)}{\partial x_j} = 0, \tag{2}$$

where ε_{ij} is the permittivity of the air, $E_i(i=1,2)$ represents the Cartesian components of the electric field $\boldsymbol{E}$, ρ_e is the charge density, μ_e is the mobility of ion and $x_i(i=1,2)$ represents the Cartesian coordinates. Here, we adopted the Einstein convention that whenever the index appeared twice in any term, we implied the summation over the range of that index. We used constant values $\varepsilon_0 = 8.85 \times 10^{-12}$ A^{2}s^4/kg m^3 and $\mu_e = 2.0 \times 10^{-4}$ m^2/V s. FLUENT uses a finite volume method to solve Eqs. (1) and (2). Charge and electric potential terms are coupled in Eqs. (1) and (2). With advancing time electric potential and charge distribution are alternately calculated until they reach a steady state. The electric current produced by corona discharge is given by the Sarma's assumption.[15] The charge density around the wire is set to keep the intensity of the electric field at threshold strength on its surface by neglecting the corona sheath. The calculated electric field is presented on the cross-section of the corona device since the shape of the corona device is assumed to be uniform along the corona wire.

An initial value for the charge density ρ_e is assumed, and then it is updated according to the following formula:

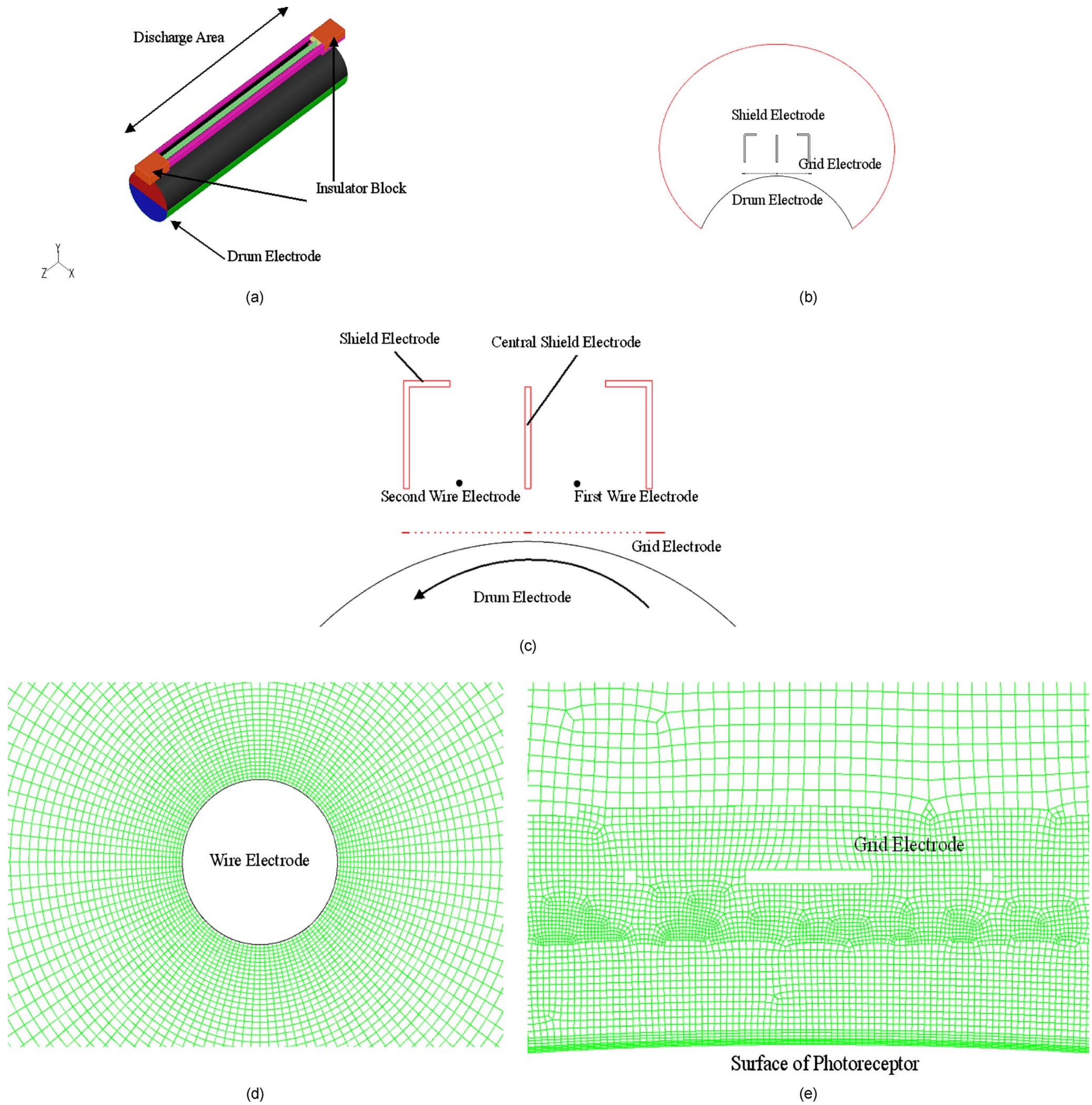

Figure 1. (a) Scorotron and photoreceptor. (b) Two-dimensional analysis model. (c) Cross-section diagram of the double-wire scorotron. (d) Computational mesh around the wire electrode. This region is divided into 120 elements in the tangential direction. (e) Unstructured computational mesh near the grid electrode. This region is discontinuously divided.

$$\rho_{e,new} = \rho_{e,old} + \alpha(E - E_0), \tag{3}$$

where α is an experimentally found coefficient, $\rho_{e,old}$ is the previous value for the charge density on the surface in the previous iteration, and $\rho_{e,new}$ is the new estimated one. Above the corona onset level, the electric field E on the wire surface should be constant and equal to the onset electric field strength $E_0 = 2.0 \times 10^7$ V/m. If this is not the case and the electric field is larger than E_0, the charge density on the wire surface is increased. Adding a charge decreases the electric field strength near the wire since the wire voltage is generally constant. If the electric field E is too small, the charge density is decreased. Subtracting a charge similarly increases the electric field strength near the wire. This process continues until the difference between E and E_0 is sufficiently small. Finally the electric field E becomes the onset electric field strength E_0. By using the user defined function[16] to consider Eq. (3), FLUENT calculates the two-dimensional steady electric field.

Under the constant current condition around the wires,

Table I. Geometrical parameters for the scorotron and the photoreceptor.

Width of corona device [m]	3×10^{-2}
Height of corona device [m]	2×10^{-2}
Length of corona device [m]	4×10^{-1}
Length of corona descharge [m]	3×10^{-1}
Width of ventilation slit [m]	2×10^{-2}
Thickness of shield electrode [m]	8×10^{-4}
Length of ventilation slit [m]	3×10^{-1}
Diameter of corona wire [m]	4×10^{-5}
Diameter of photoreceptor [m]	8×10^{-2}
Space between grid and photoreceptor [m]	1×10^{-3}
Thickness of charge transport layer [m]	2×10^{-5}

Table II. Electrical parameters for the scorotron and the photoreceptor

Wire voltage [V]	−4000 ~ −6000
Shield voltage [V]	−700
Grid voltage [V]	−700
Photoreceptor voltage [V]	0

corona discharge simulation was carried out. We used Muller's method[17] to control the constant current around the wires. Besides, we determine the static electric potential on the surface of the photoreceptor from the surface charge density. We show numerical results for a constant current of 700 μA. The contours of the electric potential are shown in Figure 2(a). The colors represent the magnitude of the electric potential [V]. The contours of the charge density are also shown in Fig. 2(b). They are colored to indicate levels of charge density [C/m^3]. [Although the text makes reference to color online, figures will appear black and white in print]. Effect of charging on the photoreceptor is small inside the scorotron. The charges between the wire and the photoreceptor are dense. The charges outside the shield case are also small. Fig. 2(c) shows the calculated distribution of the photoreceptor surface voltage. In this figure, the left and right edges of the scorotron are 0.040 and 0.075 m, respectively. We will discuss[18] the solution accuracy and show that this system is physically simple.

We first calculated the body force with the two-dimensional corona discharge simulation. Next, FLUENT can numerically predict the flow field by considering the body force as the volumetric source term of the momentum equation.

FLUENT numerically solves the Navier-Stokes equations,

$$\frac{\partial \rho}{\partial t}+\frac{\partial(\rho u_j)}{\partial x_j}=0, \tag{4}$$

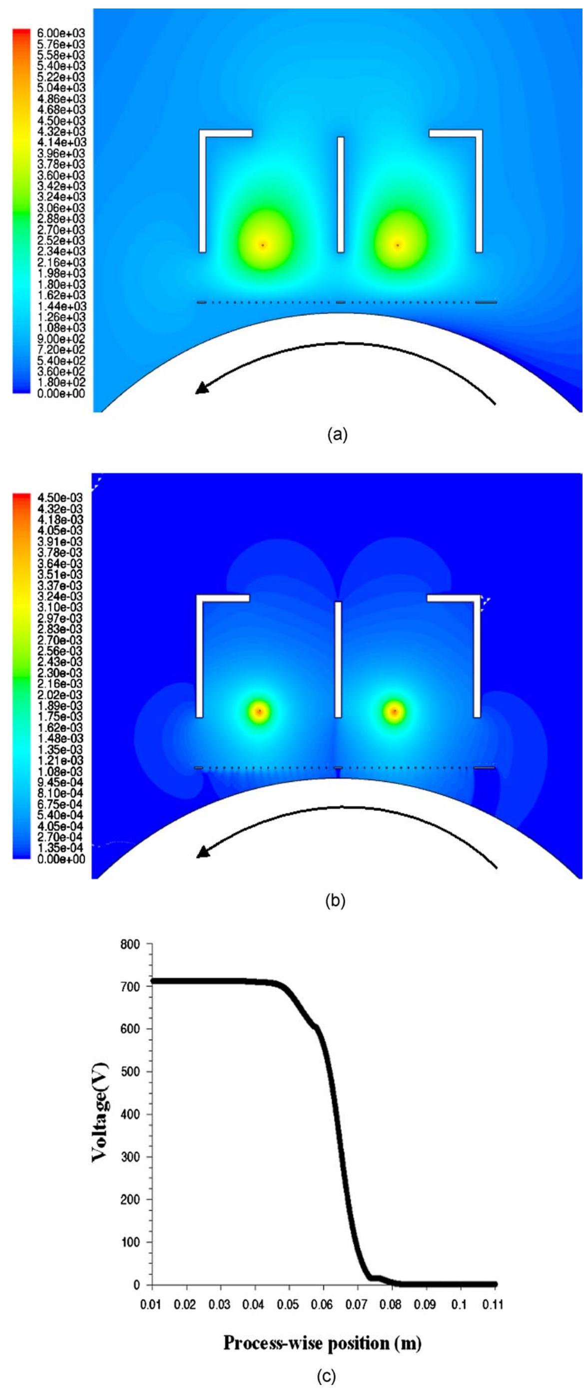

Figure 2. (a) Calculated contours of static electric potential on corona discharge. (b) Calculated contours of charge density on corona discharge. (c) Calculated distribution of static electric potential on the surface of the photoreceptor. The left and right edges of the scorotron are 0.040 and 0.075 m, respectively.

$$\frac{\partial(\rho u_i)}{\partial t}+\frac{\partial(\rho u_i u_j)}{\partial x_j}=-\frac{\partial p}{\partial x_i}+\frac{\partial}{\partial x_j}\left(\mu\frac{\partial u_i}{\partial x_j}\right)+F_i, \tag{5}$$

$$F_i=\rho_e E_i, \tag{6}$$

where ρ is the fluid density, p is the static pressure, $u_i(i=1,2)$ represents the Cartesian components of velocity $\boldsymbol{u}$, $F_i(i=1,2)$ represents the Cartesian components of the body force derived from the ionic wind and μ is the molecular viscosity of the fluid. We used constant values $\rho=1.204$ kg/m^3 and $\mu=1.808\times10^{-5}$ kg/m s. It is reasonable to assume that the fluid is incompressible. Equation (6) is not necessarily accurate as the static electric force is not fully converted to the driving force for neutral particles.

The calculation mesh around the wire electrode is very fine because the electric potential and charge distribution change drastically there. The mesh interval is set up the minimum value of 0.8 μm in the wire vicinity. The body force is radial from the wire. The body force is strong between the wire and the photoreceptor. In contrast, the body force is weaker in the upper ventilation slit. By using the user defined function[16] to capture the body force as the volumetric source term, FLUENT calculates the two-dimensional steady flow field. We monitored flow rate at the ventilation slit of the scorotron with the residuals for a convergence check. In this case, we could get steady-state solutions.

TWO-DIMENSIONAL FLOW FIELD BY TRACER PARTICLES ON NEGATIVE CORONA DISCHARGE

Particle imaging velocimetry (PIV) was applied to measure the ionic wind around a wire electrode in the previous papers.[7,9] We sequentially show the flow field by tracer particles in Figures 3(a)–3(c) on negative corona discharge. Smoke from an incense stick was used to provide the tracer particles; average diameter of these particles is about 0.2 μm. We use this value as the representative diameter of smoke particles. The voltage of the first wire and the voltage of the second wire, are set at -4500 and -5400V, respectively. Fig. 3(a) shows the initial flow field on negative corona discharge by tracer particles. A long envelope region has already appeared around the second wire. Particles keep away from the wire and cannot penetrate this region. An elliptic region appears around the first wire. Fig. 3(b) shows the flow field by tracer particles after 10^{-4} s. The elliptic region spreads around the first wire. Fig. 3(c) shows the flow field by tracer particles after next 10^{-4} s. The elliptic region decays around the first wire. These regions transiently behave in ways swaying from right to left in the ionic wind.

MOTION OF SMOKE PARTICLES AROUND A WIRE ON NEGATIVE CORONA DISCHARGE

From the above observations we may qualitatively analyze the motion of charged particles around wires. At first, Figure 4(a) shows contours of velocity magnitude in the neighborhood of the scorotron. The contours are colored to indicate levels of the velocity magnitude [m/s]. Figure 4(b) also shows contours of static pressure (gauge pressure) on corona discharge. The contours are colored to indicate levels of static pressure [Pa]. The Reynolds number around the wire $R_e=5.3$ is sufficiently small, and the flow field is laminar. We defined a reference velocity $U=2$ m/s and a reference length $L=40$ μm. It is reasonable to assume that the flow

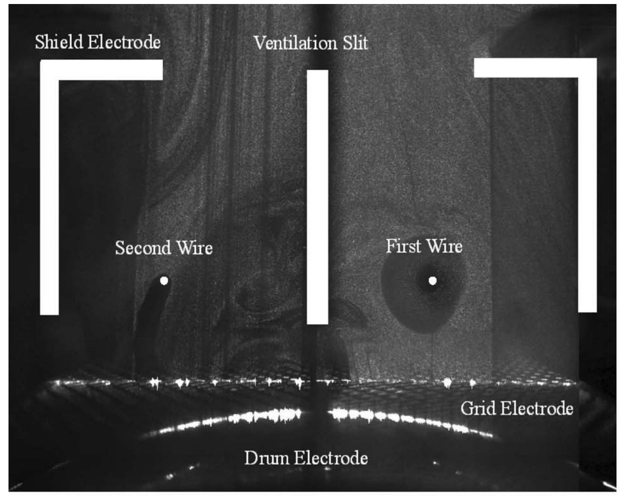

(a)

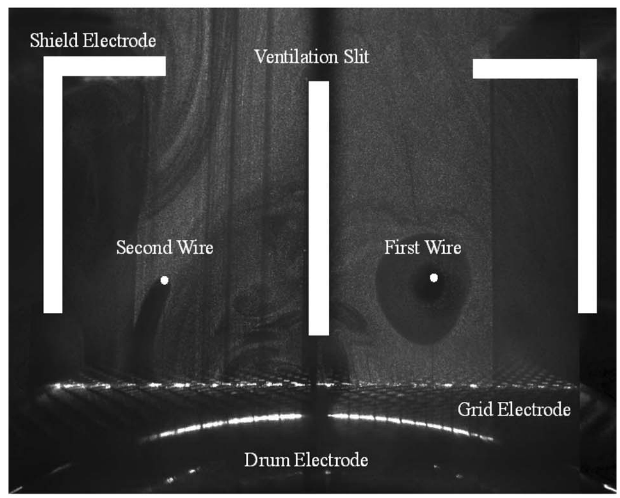

(b)

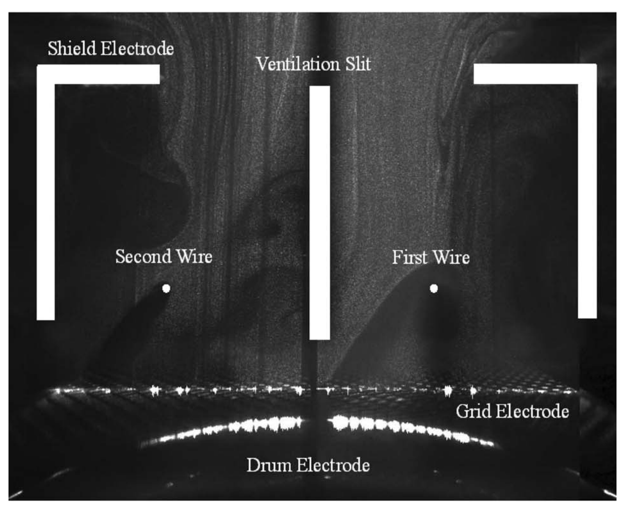

(c)

Figure 3. (a) Initial flow field on negative corona discharge by tracer particles. A long envelope region has already appeared around the second wire and an elliptic region appears around the first wire. (b) Flow field by tracer particles after 10^{-4} s. The elliptic region spreads around the first wire. (c) Flow field by tracer particles after next 10^{-4} s. The elliptic region decays around the first wire.

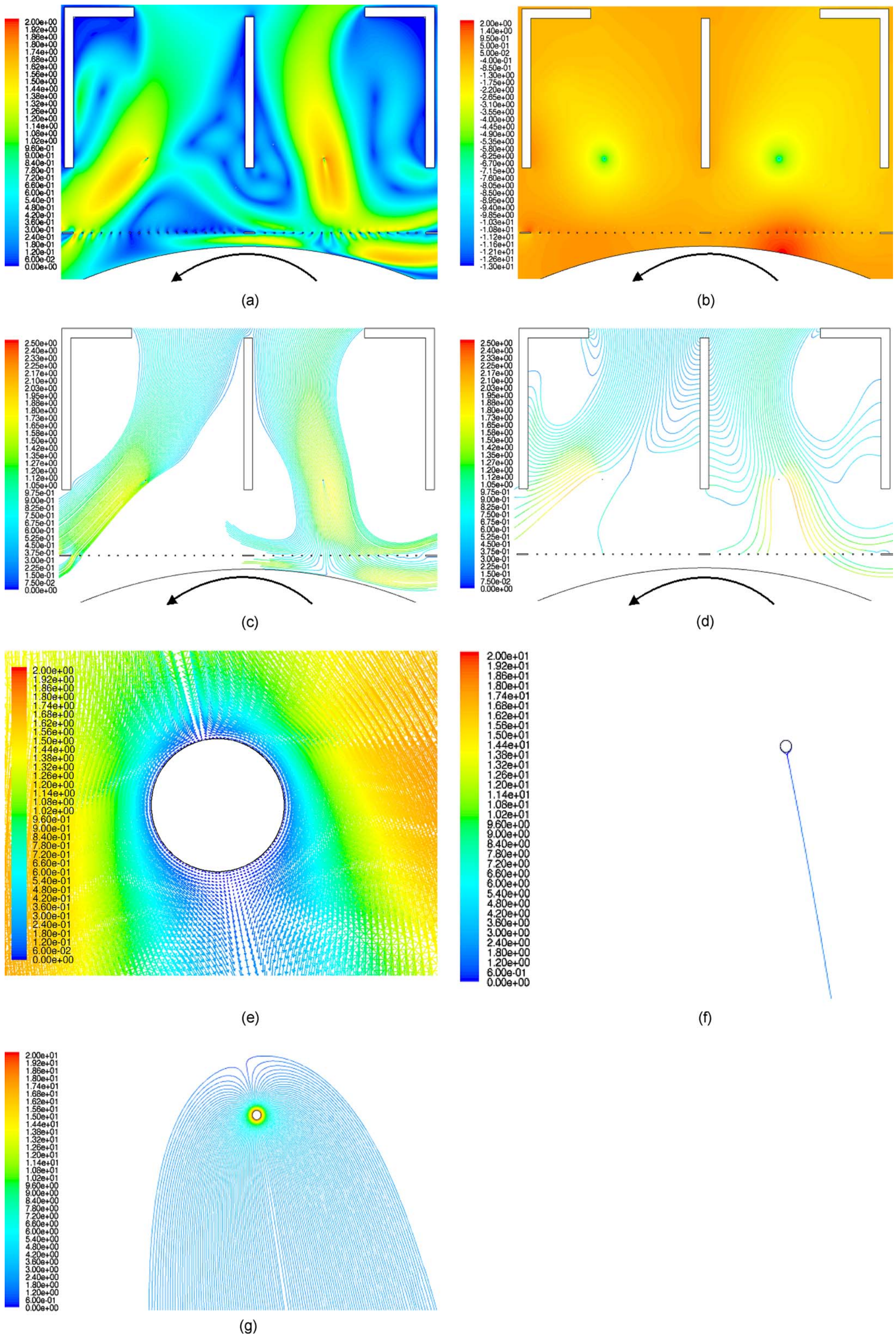

Figure 4. (a) Calculated contours of velocity magnitude on corona discharge. (b) Calculated contours of static pressure on corona discharge. (c) Calculated behavior of uncharged smoke particles with a diameter of 0.2 μm. They are ejected from the surface of the ventilation slit. (d) Calculated behavior of charged smoke particles. They are ejected from the surface of the ventilation slit. The particle charge is 2×10^{-15} C for particles with a diameter of 0.2 μm. (e) Calculated velocity vectors around the first wire. (f) Calculated behavior of uncharged smoke particles around the first wire. Particles with a diameter of 0.2 μm are ejected from a surface of the first wire. (g) Calculated behavior of charged smoke particles around the first wire. Particles are ejected from a surface of the first wire. The particle charge is 2×10^{-15} C for a particle with a diameter of 0.2 μm.

field is laminar. A flow rate through the ventilation slit is 2×10^{-2} kg/s per unit length. Airflow is mainly induced by corona discharge. The λ-shaped flow is generated at the first wire side same as a single-wire scorotron[7] and flow separations occur in the scorotron. Our numerical calculations correlate well with these experimental results. However, the flow field below the central shield electrode is different from the three-dimensional flow field.[9] The grid electrode has a three-dimensional pattern.

Next we show the calculated behavior of the particles. An aerosol is a two-phase medium that can be composed of solid particles or liquid droplets in the gas phase. It is well known that two mechanisms[19] of aerosol particle charging are distinguished: field and diffusion charging. In field charging ions are accelerated toward the particle by the external electric field. The particle is charged by the ions up to the point where the charge on the particle becomes a source of such a strong electric field that it prevents subsequent ions from reaching the particle surface. In diffusion charging the movement of ions is due to their thermal energy. Only the ions of sufficiently high energy collide with the particles. The field mechanism dominates for particles larger than 1 μm in diameter, while for particles smaller than 0.1 μm in diameter, the diffusion mechanism is dominant. In the intermediate region, both mechanisms contribute to charging. Since charging the particle by ion diffusion is independent of the external electric field but depends only on the field due to the particle charge, field charging is dominant around wires. As we could not find any evidence of random motion in the smoke particles around the corona wire, we assumed that charged smoke particles mainly respond to the effect of a background electric field. We also assumed that the field charging is dominant for particles with a diameter of 0.2 μm. We have not considered the role of the negative ions of sufficiently high energy, and therefore we treat only the motion of charged particles in Eqs. (1)–(6). Hence, interaction among the other particles is ignored.

FLUENT[20,21] predicts the trajectory of a discrete phase particle by integrating the balance for the particle, which is written in a Lagrangian reference frame. This force balance equates the particle inertia with the forces acting on the particle, and can be written as

$$\frac{d\vec{u}_p}{dt} = F_D(\vec{u} - \vec{u}_p) + \frac{\rho_p - \rho}{\rho_p}\vec{g} + \vec{F}, \tag{7}$$

$$F_D = \frac{18\mu}{\rho_p D_p^2}\frac{C_D R_e'}{24}, \tag{8}$$

where the first term to the right of Eq. (7) is drag force per particle, the second term is buoyancy and the third term is additional forces. Additional forces contain the virtual mass force, or force excited due to the pressure gradient. These forces are ignored because droplet density is much greater than air density in this analysis. The electric force that multiplies the particle charge and the electric field together is defined instead. Here, $\boldsymbol{u_p}$ is the particle velocity, ρ_p is the density of the particle, and D_p is the particle diameter. R_e' is the relative Reynolds number and C_D is the drag coefficient. We show the behavior of charged particles whose diameter is 0.2 μm in Fig. 4(c), where we have defined the particle density as $\rho_p = 300$ kg/m^3. We qualitatively show the behavior of charged particles in Fig. 4(d), where color indicates the magnitude of the particle velocity [m/s]. We set a constant particle charge of 2×10^{-15} C for particles with a diameter of 0.2 μm. Particles keep away from the wire. Figure 4(e) shows calculated velocity vectors around the first wire. The flow field is consistent with one[3] modeled by Yoshizawa and co-workers.

Figures 4(f) and 4(g) show the calculated behavior of uncharged particles and the calculated behavior of charged particles, respectively. Particles are repelled from the surface of the first wire. We do not find any evidence clearly related to the envelope region in Fig. 4(f). On the other hand, the envelope in Fig. 4(g) occurs at the boundary of the long region. Charged particles cannot exist in this region. By comparing the behavior of these particles with Figs. 3(a)–3(c), we can conclude that the electrostatic field governs the behavior of charged particles around a wire.

DISCUSSION

We have investigated the characteristics of the ionic wind in a double-wire scorotron. In this section, we especially discuss the motion of charged particles around a wire on corona discharge by comparing the initial flow field with numerical steady-state solutions. Figure 5(a) shows a schematic of the motion of a charged particle just after the beginning of corona dicharge. The particles are repelled by the electron emission. Figure 5(b) also shows a schematic diagram of motion of a charged particle around the second wire just after onset of the ionic wind. As the ionic wind increases, a long envelope region appears.

Lastly, we consider the particle charge which depends on particle location. Above, we qualitatively showed the motion of constant charged particles around wires. The saturation charge[19] is given by

$$3\pi\varepsilon_0\frac{\varepsilon_r}{\varepsilon_r + 2}D_P^2 E, \tag{9}$$

where ε_r is the relative dielectric constant of particles. We can get the saturation charge 4×10^{-17} C for a particle with a diameter of 0.2 μm for the onset electric field strength E_0. However, compared to the maximum saturation charge 4×10^{-17} C of a particle with a diameter of 0.2 μm, the constant particle charge of 2×10^{-15} C is too large. Therefore, we define the particle charge for a particle with a diameter of 0.2 μm by the following relation:

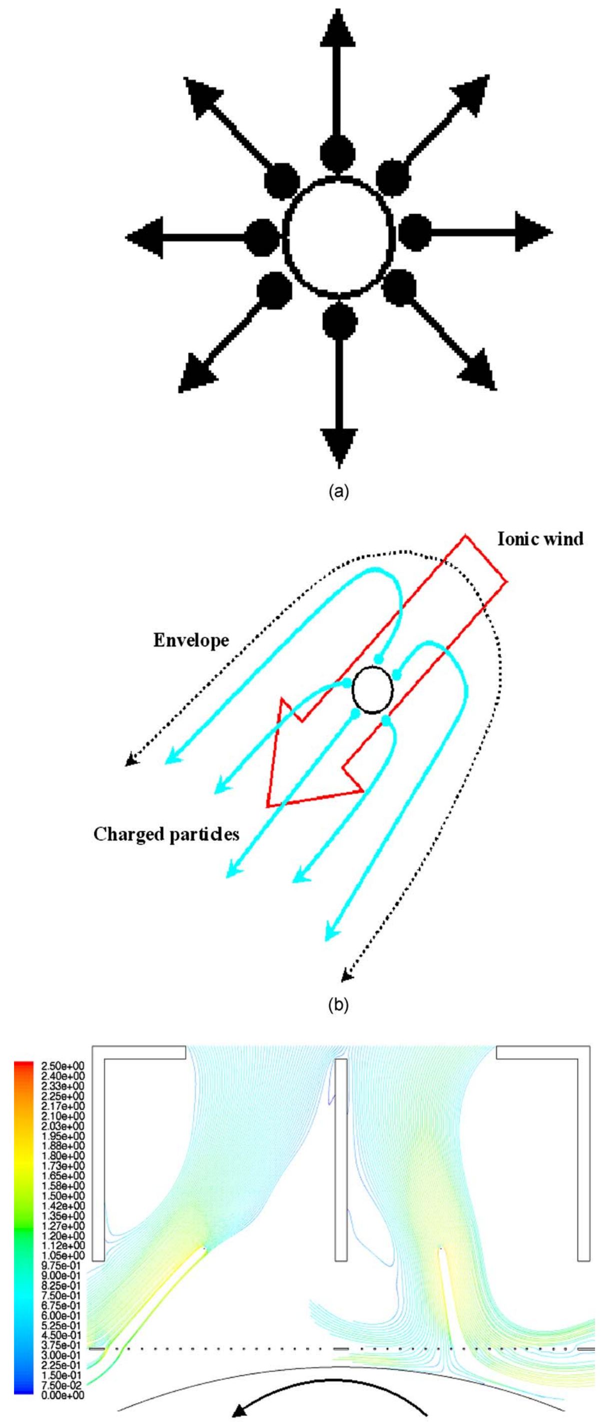

Figure 5. (a) Schematic of motion of a charged particle around a wire just after the beginning of negative corona discharge. (b) Schematic of motion of a charged particle around the second wire just after the occurrence of the ionic wind. (c) Calculated behavior of charged smoke particles with a diameter of 0.2 μm. The particle charge is defined by Eq. (10).

$$3\pi\varepsilon_0 \frac{\varepsilon_r}{\varepsilon_r + 2} D_P^2 E \frac{t}{t + \dfrac{4\varepsilon_0}{\mu_e \rho_e}}, \tag{10}$$

where t is time, and we require that particle charge does not decrease with time. Equation (10) is based[22] on Cochet's analytical solution. Generally, the electrical field strength is a local function and therefore this influences the particle saturation charge. However, these local functions have not been considered in common models. Parker described that such a solution becomes possible[22] only when particle trajectories are calculated.

We show the behavior of charged particles whose charge is defined by Eq. (10) in Fig. 5(c). The electrical field strength is defined as a local function $E = E(x,y)$ in Eq. (10). In Eq. (10), $t=0$ is set at the ventilation slit. For most dielectric substances, ε_r is less than 10. We assumed a constant value $\varepsilon_r = 3$ for smoke particles. In Fig. 5(c) color represents the magnitude of the particle velocity [m/s].

As the effect of the electric field is negligible on the region far away from the wires, the thickness of the envelope region is significant. The thickness for the smoke particles with an average diameter of 0.2 μm is about 1 mm. FLUENT shows the particle charge in the calculation of particle trajectories. The charge is really about 6×10^{-18} C for particles for a diameter of 0.2 μm though maximum saturation charge is 4×10^{-17} C for the onset electric field strength $E_0 = 2.0 \times 10^7$ V/m. The estimate becomes smaller since the electric field decreases away from a wire.

It is well known that smoke particles are positively charged by combustion. Smoke particles generally keep away from the wires on corona discharge in spite of the polarization of the wires. If positively charged particles can exist in a scorotron, the electrons or negative ions gravitate toward them due to the perturbed electric field. So we estimate that larger particles in an airflow behave as smoke particles in the scorotron on corona discharge. On the other hand, the particles collide with the grid electrode. This phenomenon is essentially the same as the electrostatic precipitator. However, we cannot adequately explain the contamination of the wire. It is well known that some chemical reactions are remarkably accelerated in a corona discharge. Therefore, we infer that chemical reactions, e.g., chemical vapor deposition (CVD), should govern the contamination of the wire on corona discharge.

SUMMARY

We have investigated the characteristics of the ionic wind in a double-wire scorotron. Especially, we have shown the motion of charged particles in the scorotron on negative corona discharge. We have discovered the following:

(i) Envelope regions into which smoke particles cannot penetrate appear. These regions transiently behave in ways swaying from right to left in the ionic wind. This transient phenomenon is significant for the contamination of the grid electrode.

(ii) Except for the immediate vicinity of the wires, our numerical calculations correlate well with our experimental results. The electrostatic effect is limited in the neighborhood of the wire.

(iii) Smoke particles are positively charged by combustion, i.e., particle charge is initially positive. Smoke particles generally keep away from the wires on corona discharge in spite of the polarization of the wires. Free mobile carriers charge smoke particles.

(iv) We estimate that the particle charge is about 6×10^{-18} C around a wire for particles with a diameter of 0.2 μm, even though maximum saturation charge is 4×10^{-17} C for the onset electric field strength $E_0=2.0\times10^7$ V/m.

As we unfortunately have no visualization method for the motion of any particles, we cannot immediately discuss the motion of any free powders. As particles with a diameter less than about 1 μm easily move on the flow, effect of the background electrostatic field is significant for the behavior of particles on corona discharge. Similarly, it is necessary that diffusion charging should be investigated for finer particles.

ACKNOWLEDGMENTS

The author would like to thank Mr. Masato Shiraishi for measurements of the flow field. The author is also grateful to Mr. Hideki Okamoto for fruitful discussions and valuable advices.

References

[1] E. M. Williams, *The Physics and Technology of Xerographic Processes* (John Wiley and Sons, New York, 1984), p. 4.

[2] A. Yabe, Y. Mori, and K. Hijikata, "EHD Study of Corona Wind between Wire and Plate Electrodes", AIAA J. **16**, 340 (1978).

[3] Y. Itoh, M. Yoshizawa, T. Tsuzuki, and M. Sugawara, "Numerical Analysis of the Fluid Field near the Corona Wire due to the Corona Discharge (The Vortex Formation and the Fluid Force on the Wire)", Trans. Jap. Soc. Mech. ENG. (C) **64**, 4115 (1998) (In Japanese).

[4] T. Yamamoto, M. Okuda, and M. Okubo, "Three-dimensional ionic wind and electrohydrodynamics of tuft/point corona electrostatic precipitator", IEEE Trans. Ind. Appl. **39**, 1602 (2003).

[5] K. Nashimoto, "Growth of Silicon Oxide and Formation of Reactive Gases Induced by Corona Discharge", Doctoral thesis, Nagoya Institute of Technology, 1989.

[6] P. Zamankhan, G. Ahmadi, and F. Fan, "Variation of Airflow and Electric Field in a Corona Device During Charging of a Moving Dielectric Substrate", J. Imaging Sci. Technol. **50**, 375–385 (2006).

[7] K. Mori, H. Okamoto, and N. Hirooka, "Computational Fluid Dynamics of Ionic Wind in a Corona Device in Electrophotography-(1)", J. Imaging Sci. Technol. **48**, 465–472 (2004).

[8] K. Mori, "Computational Fluid Dynamics of Precision Machinery Design", Doctoral thesis, Osaka City University, 2005, pp. 27–46.

[9] K. Mori, H. Okamoto, M. Shiraishi, and A. Nishimura, "Computational Fluid Dynamics of Ionic Wind in a Corona Device in Electrophotography-(2)", J. Imaging Sci. Technol. **53**, 040502.1–040502.8 (2009).

[10] M. Scharfe, *Electrophotography Principles and Optimization* (John Wiley and Sons, New York, 1984), p. 7.

[11] K. Otsuka and M. Shiraishi, "An Analysis of Corotron Wire Break", *Proceedings of Reliability and Maintainability Symposium JUSE* (2005) p. 15 (In Japanese).

[12] Fuji Xerox Co, Ltd., DocuCentre f1100/900 a1100/900, *Fuji Xerox Technical Report No. 15*, 95(2005), (In Japanese).

[13] I. Shiga, Y. Itoh, M. Yoshizawa, and T. Sugiura, "Self-Excited Lateral Oscillation of a Wire Electrode due to Corona Discharge (the ionic flow near the wire electrode)", *Proceedings of The 19th Symposium on Electromagnetics and Dynamics (SEAD19)* (2007) p. 177 (In Japanese).

[14] Y. Zhou, T. Seki, S. M. Somasiri, K. K. C. Kumar, and Y. Hoshino, "Observation of Particle Motion between Voltage Applied Electrodes", J. Imaging. Soc. Japan **44**, 445 (2005) (In Japanese).

[15] M. P. Sarma and W. Janischewskyj, "DC corona on smooth conductors in air", Proc. IEEE **116**, 161 (1969).

[16] Fluent Inc., FLUENT 6.0 UDF Manual, 2001.

[17] J. H. Mathews and K. D. Fink, *Numerical Methods Using Matlab*, 4th ed., (Prentice-Hall Inc., Englewood Cliffs, NJ, 2004) p. 92.

[18] K. Mori, Y. Nagamori, K. Otsuka, H. Okamoto, and T. Ito, "Unstructured Finite Volume Method of Electric Field in a Scorotron", J. Imaging. Soc. Japan. **49**, 248 (2010) (In Japanese).

[19] P. H. F. Liu and B. G. Liptak, *Environmental Engineers' Handbook*, 2nd ed. (Lewis Publishers, Boca Raton, FL, 1997) p. 356.

[20] K. Mori, "Computational Fluid Dynamics of Dispersed Mist Phenomenon in a Thermal Ink Jet Printer", J. Imaging Sci. Technol. **47**, 250–255 (2003).

[21] M. Fujii and K. Mori, "Analysis on Behavior of Small Ink Drops Ejected from Ink Jet Printhead", J. Imaging. Soc. Japan. **48**, 244 (2009) (In Japanese).

[22] K. R. Parker, *Applied Electrostatic Precipitation* (Blackie Academic and Professional, London, UK, 1997), p. 53.